

Protein electron transfer: a numerical study of tunneling through fluctuating bridges

Qian Xie¹, Georgios Archontis, Spiros S. Skourtis^{*}

Department of Natural Sciences, University of Cyprus, Nicosia 1678, Cyprus

Received 23 April 1999

Abstract

A central challenge of protein electron-transfer theory is to understand how the protein dynamics influences the electron tunneling from donor to acceptor. It is shown that tunneling (as a function of time) through a fluctuating protein bridge is drastically different from tunneling through a chemically identical static bridge. The static two-state approximation that leads to the donor–acceptor matrix element T_{DA} , is therefore inadequate. A time-dependent two-state approximation is found that describes the tunneling dynamics through a fluctuating bridge. The fluctuating system electronic Hamiltonians are constructed from molecular dynamics trajectories at the CNDO-SCF level. © 1999 Elsevier Science B.V. All rights reserved.

1. Introduction

Electron-transfer (ET) reactions are important components of chemical and biological processes [1–3]. In a typical reaction, an electron tunnels from a localized donor orbital (D) to a localized acceptor orbital (A) located several Ångströms away from D. Tunneling is mediated by the intervening medium between D and A (the bridge). The ET rate is given by the nonadiabatic expression [1,3]

$$K_{D \rightarrow A} = \frac{2\pi}{\hbar} T_{DA}^2(\text{FC}). \quad (1)$$

(FC) is the Franck–Condon overlap factor between D and A vibronic manifolds. T_{DA} is the bridge-mediated

tunneling matrix element between D and A electronic wavefunctions [4]. The reliable computation of T_{DA} is central to the field of protein-mediated electron transfer [2], where one of the main challenges is to understand how a protein structure influences electronic tunneling [3,5]. Traditionally, T_{DA} is computed using static protein structures (obtained from X-ray crystallography and energy minimization). In recent years, several researchers [6–12] have concluded that the dynamics of the protein structure should be incorporated in the analysis of T_{DA} . We address this issue by comparing, as a function of time, tunneling through a fluctuating protein bridge to tunneling through a chemically identical static bridge. We first compute the probability of electron transfer through a fluctuating β -sheet structure (Fig. 1) for several pairs of D–A orbitals chosen to cover different sections of the sheet. Then we compute the ET probability for the static structure, using the same D–A pairs as before. The two

^{*} Corresponding author. Fax: +35-7-2-33-90-60; e-mail: skourtis@elgreco.ns.ucy.ac.cy

¹ Supported by the University of Cyprus.

B-SHEET (azurin)

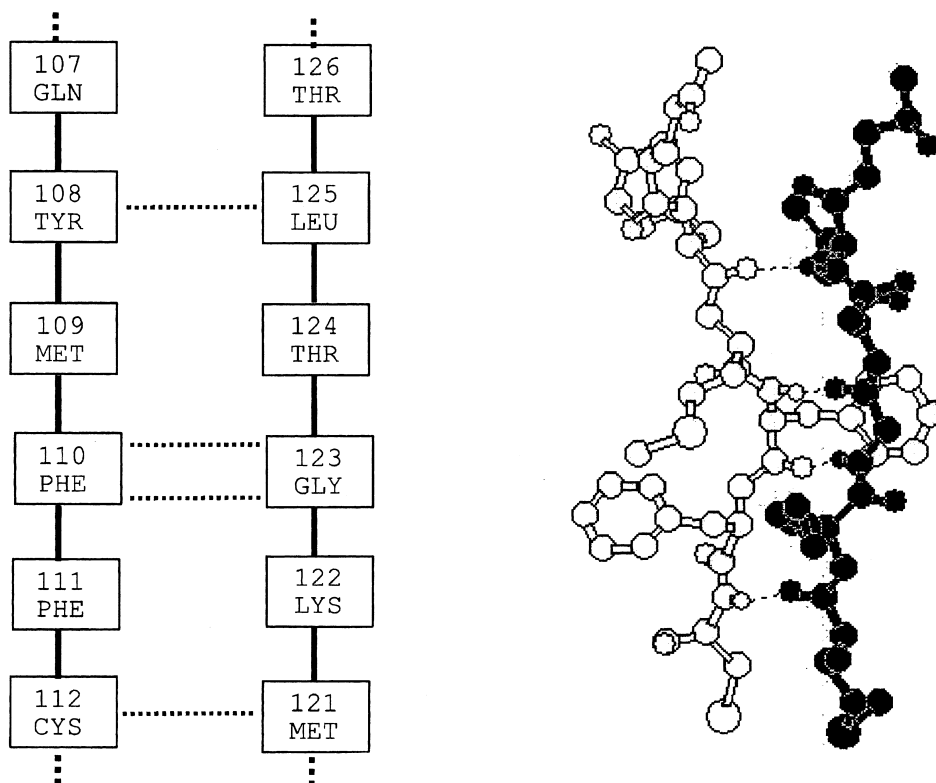


Fig. 1. The β -sheet of azurin [13] formed by strands 7 and 8. Electron transfer through this sheet has been studied experimentally and theoretically [19]. There are four hydrogen bonds between the two strands.

sets of probabilities are compared and it is shown that they can differ considerably. A question that immediately arises is whether there exists an analogue of the static two-state approximation that describes the ET probability through the fluctuating bridge. We show how to construct a time-dependent effective two-state Hamiltonian that approximates well this probability for long times. As in the static case, the off-diagonal element of such a Hamiltonian, $T_{DA}(t)$, describes ET pathways (that change with time). In contrast to the static case, it is necessary to use a time-dependent tunneling energy for the construction of the two-state Hamiltonian. Further-

more, the effective diagonal matrix elements, $T_{DD}(t)$ and $T_{AA}(t)$, are as important as $T_{DA}(t)$ for the description of tunneling; they alter the level crossing dynamics within the two-state approximation.

2. Overview of calculations

The starting point of all calculations here is the time-dependent Schrödinger equation of the fluctuating donor–bridge–acceptor system, $i\hbar d|\Psi(t)\rangle/dt = \hat{H}(t)|\Psi(t)\rangle$. $\hat{H}(t)$ ($|\Psi(t)\rangle$) is the one-particle Hamiltonian (state) of the transferring electron or

hole. In terms of donor–acceptor (D–A) and bridge (br) subspaces,

$$\hat{H}(t) = \hat{H}_{\text{DA}}(t) + \hat{H}_{\text{br}}(t) + \hat{H}_{\text{DA-br}}(t), \quad (2)$$

where

$$\begin{aligned} \hat{H}_{\text{DA}}(t) &= |\phi_{\text{D}}\rangle E_{\text{D}}\langle\phi_{\text{D}}| + |\phi_{\text{A}}\rangle E_{\text{A}}\langle\phi_{\text{A}}| \\ &\quad + (|\phi_{\text{D}}\rangle V_{\text{DA}}\langle\phi_{\text{A}}| + \text{h.c.}), \\ \hat{H}_{\text{br}}(t) &= \sum_i |\phi_i^{\text{br}}\rangle E_i^{\text{br}}\langle\phi_i^{\text{br}}| \\ &\quad + \sum_{i>j} (|\phi_i^{\text{br}}\rangle V_{ij}^{\text{br}}\langle\phi_j^{\text{br}}| + \text{h.c.}), \\ \hat{H}_{\text{DA-br}}(t) &= \sum_i (|\phi_{\text{D}}\rangle V_{\text{Di}}\langle\phi_i^{\text{br}}| + \text{h.c.}) \\ &\quad + \sum_i (|\phi_{\text{A}}\rangle V_{\text{Ai}}\langle\phi_i^{\text{br}}| + \text{h.c.}). \end{aligned} \quad (3)$$

In the above equations, ϕ_{D} , ϕ_{A} , and $\{\phi_i^{\text{br}}\}$ denote time-dependent D, A, and bridge orbitals which follow the molecular fluctuations. All orbital site-energies E_i and all inter-orbital couplings V_{ij} are time-dependent. Details of the CNDO-SCF computation of $\hat{H}(t)$ from molecular dynamics (MD) trajectories are given in the next section.

In matrix form, the Schrödinger equation is

$$i\hbar \frac{d}{dt} \Psi(t) = [\mathbf{H}(t) - i\hbar\mathbf{K}(t)] \Psi(t), \quad (4)$$

if at each time t the basis is orthonormalized, $\langle\phi_i(t)|\phi_j(t)\rangle = \delta_{ij}$. $\mathbf{H}(t)$ is the Hamiltonian matrix of the system $H_{ij}(t) = \langle\phi_i(t)|\hat{H}(t)|\phi_j(t)\rangle$, and $K_{ij}(t) = \langle\phi_i(t)|d\phi_j(t)/dt\rangle$. $\Psi(t)$ denotes the state vector of the system,

$$\begin{aligned} \Psi(t) &= \begin{pmatrix} C_{\text{D}}(t) \\ C_{\text{br1}}(t) \\ \vdots \\ C_{\text{brN}}(t) \\ C_{\text{A}}(t) \end{pmatrix} \quad \text{where } C_i(t) \\ &= \langle\phi_i(t)|\Psi(t)\rangle. \end{aligned} \quad (5)$$

For a particular D–A pair, the quantity of interest is the ET probability

$$P_{\text{DA}}(t) = |\langle\phi_{\text{A}}(t)|\Psi(t)\rangle|^2$$

where

$$|\Psi(0)\rangle = |\phi_{\text{D}}(0)\rangle. \quad (6)$$

In terms of the $\Psi(t)$ components, $P_{\text{DA}}(t) = |C_{\text{A}}(t)|^2$ given $C_i(0) = \delta_{i\text{D}}$.

The first stage of our calculations (Fig. 2) involves the computation of the probability in Eq. (6) using $\mathbf{H}(t)$ of the entire β -sheet in Eq. (4). In order to probe pathways that traverse several different segments of the β -sheet, we must use artificial D–A pairs located at many different positions along the sheet. We choose C_{α} –H bond orbitals as D–A pairs and, to ensure tunneling mediation for all times, $E_{\text{D}}(t)$ and $E_{\text{A}}(t)$ are shifted by a constant energy into the HOMO–LUMO gap of the bridge (Fig. 2). In order to isolate effects arising from bridge motion from effects arising from the dynamics of E_{D} and E_{A} , two sets of calculations are carried out at this stage. In one set (top of Fig. 2), the time-dependencies of $E_{\text{D}}(t)$ and $E_{\text{A}}(t)$ are retained, and $E_{\text{D}}(t)$, $E_{\text{A}}(t)$ cross each other frequently. In the other set (bottom of Fig. 2), the D and A energies are set equal to their initial values for all times, thus avoiding D–A level crossings. For each case (fluctuating and static E_{D} , E_{A}), we compare tunneling through the dynamic bridge ($P_{\text{DA}}(t)$ or $\mathcal{P}_{\text{DA}}(t)$, respectively, in Table 1) to tunneling through a chemically identical static bridge ($P_{\text{DA}}^{\text{st}}(t)$ or $\mathcal{P}_{\text{DA}}^{\text{st}}(t)$, respectively, in Table 1). Differences between the dynamic- and static-bridge probabilities show how rapidly the static tunneling behaviour is lost in the presence of bridge dynamics. The above comparisons are carried out among probabilities that involve identical D–A pairs, MD trajectories, and initial conditions. Furthermore, $E_{\text{D}}(0)$ and $E_{\text{A}}(0)$ are always tuned to resonance as follows. For a given trajectory, we use Eq. (4) with $\mathbf{H}(t) = \mathbf{H}(0)$ to compute the ET probability for the static system frozen at its initial conformation, i.e., $\mathcal{P}_{\text{DA}}^{\text{st}}(t) = |\langle\phi_{\text{A}}(0)|\Psi(t)\rangle|^2$ with $|\Psi(0)\rangle = |\phi_{\text{D}}(0)\rangle$, and then we find values of $E_{\text{D}}(0)$ and $E_{\text{A}}(0)$ such that $\mathcal{P}_{\text{DA}}^{\text{st}}(t) \approx \sin^2(\Omega t)$. This behaviour is characteristic of static two-state tunneling with $T_{\text{DA}} = \hbar/\Omega$.

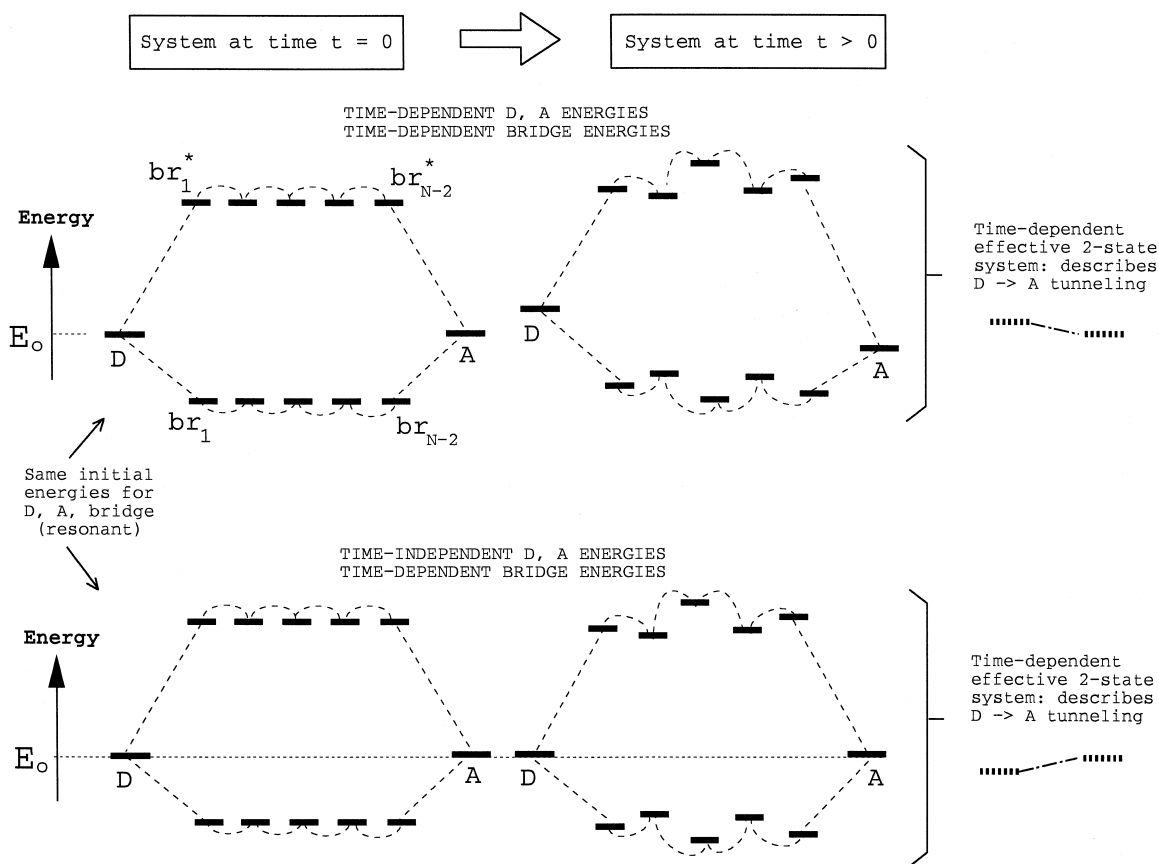


Fig. 2. Diagram showing the two sets of calculations carried out for each D–A pair and MD trajectory (see Table 1). At $t = 0$ E_D and E_A are tuned to resonance inside the HOMO–LUMO energy gap. In one set of calculations, E_D and E_A are allowed to fluctuate for $t > 0$, as dictated by MD (top). In the other set, they are kept constant for $t > 0$ (i.e. resonant, bottom). The calculations are done in two stages. In the first stage, we use $N \times N$ Hamiltonians (N : total number orbitals) to compute the D \rightarrow A ET probability for: (i) the static bridge frozen at its $t = 0$ conformation, (ii) the dynamic bridge. In the second stage, we construct 2×2 Hamiltonians that reproduce the previously computed dynamic-bridge ET probabilities. In the diagrams, br_i (br_i^*) denotes the i th bridge bond (antibond).

In the second stage of our calculations (right side of Fig. 2), we construct time-dependent 2×2 Hamil-

tonians that approximate the dynamic-bridge probabilities ($P_{DA}(t)$ or $\mathcal{P}_{DA}(t)$). To approximate $P_{DA}(t)$,

Table 1

Probabilities computed for each D,A pair and MD trajectory (refer to Eqs. (2) and (7))

	$\hat{H}_{br}(t) + \hat{H}_{DA-br}(t)$	$\hat{H}_{br}(0) + \hat{H}_{DA-br}(0)$
$\hat{H}_{DA}(t)$	$E_D(t), E_A(t)$, dynamic bridge: $P_{DA}(t)$ $\hat{H}^{2s}(t, E_{tun})$, constant E_{tun} : $P_{DA}^{dy2s}(t)$ $\hat{H}^{2s}(t, E_{tun})$, variable E_{tun} : $\tilde{P}_{DA}^{dy2s}(t)$	$E_D(t), E_A(t)$, static bridge: $P_{DA}^{st}(t)$
$\hat{H}_{DA}(0)$	$E_D(0), E_A(0)$, dynamic bridge: $\mathcal{P}_{DA}(t)$ $\hat{H}^{2s}(t, E_{tun})$, constant E_{tun} : $\mathcal{P}_{DA}^{dy2s}(t)$ $\hat{H}^{2s}(t, E_{tun})$, variable E_{tun} : $\tilde{\mathcal{P}}_{DA}^{dy2s}(t)$	$E_D(0), E_A(0)$, static bridge: $\mathcal{P}_{DA}^{st}(t)$ Used to tune $E_D(0)$ and $E_A(0)$ to resonance for all calculations shown in table

$\hat{H}(t)$ is projected at each time t onto $\phi_D(t)$ and $\phi_A(t)$. The resulting Hamiltonian is

$$\begin{aligned} \hat{H}^{2s}(t, E_{\text{tun}}) &= |\phi_D(t)\rangle [E_D(t) + T_{DD}(t)] \langle \phi_D(t)| \\ &+ |\phi_A(t)\rangle [E_A(t) + T_{AA}(t)] \langle \phi_A(t)| \\ &+ |\phi_D(t)\rangle [V_{DA}(t) + T_{DA}(t)] \langle \phi_A(t)| + \text{h.c.} \end{aligned} \quad (7)$$

where

$$T_{KL}(t) = \sum_{ij} V_{Ki}(t) G_{ij}^{\text{br}}(E_{\text{tun}}, t) V_{jL}(t),$$

$$K(L) = D, A \quad (8)$$

and $G_{ij}^{\text{br}}(E_{\text{tun}}, t) = \langle \phi_i^{\text{br}}(t) | (E_{\text{tun}} - \hat{H}^{\text{br}}(t))^{-1} | \phi_j^{\text{br}}(t) \rangle$ is the energy-domain bridge Green function (E_{tun} is the tunneling energy). This Hamiltonian is used in a 2×2 Schrödinger equation $i\hbar d|\Psi(t)\rangle/dt = \hat{H}^{2s}(t, E_{\text{tun}})|\Psi(t)\rangle$ to compute an approximate ET probability $|\langle \phi_A(t) | \Psi(t) \rangle|^2$. This construction is denoted the ‘dynamic two-state approximation’. If a constant E_{tun} is used in Eq. (7), the approximate probability is denoted $P_{DA}^{\text{dy}2s}(t)$. If E_{tun} is varied as a function of time, the approximate probability is denoted $\tilde{P}_{DA}^{\text{dy}2s}(t)$ (Table 1). To approximate $\mathcal{P}_{DA}(t)$, we set $E_D(t) = E_D(0)$ and $E_A(t) = E_A(0)$ in Eq. (7). In this case, the approximate probabilities for constant and time-varying E_{tun} are denoted $\mathcal{P}_{DA}^{\text{dy}2s}(t)$ and $\tilde{\mathcal{P}}_{DA}^{\text{dy}2s}(t)$ respectively (Table 1).

2.1. Computational details

The system employed consists of an azurin molecule [13] solvated by a layer of water molecules with minimum thickness of 7 Å. MD simulations are performed on the whole protein–water system with the program CHARMM [14]. The system is first equilibrated for 300 ps using the Verlet algorithm; the initial 50 ps employes a Langevin dynamics protocol. After equilibration, several dynamics segments with duration of at least 1 ps are chosen from a production trajectory. For each segment, conformational snapshots of the β -sheet portion formed by β -strands 7 and 8 (Fig. 1) are stored at 1 fs intervals. These snapshots are then used to compute the elec-

tronic Hamiltonian matrix of the entire β -sheet, $\mathbf{H}(t)$ in Eqs. (2) and (4). For times coinciding with snapshots, $\mathbf{H}(t)$ is the set $\{\mathbf{H}\}$ of all Hamiltonian matrices obtained from the snapshots of the β -sheet. Each matrix \mathbf{H} is calculated at the CNDO-SCF level and is expressed in a basis $\{\phi_i(t)\}$ of natural lone pairs and bonding/antibonding two-center orbitals, using a modified version of the BONDO program [15]. For times between snapshots, $\mathbf{H}(t)$ is obtained from $\{\mathbf{H}\}$ via cubic spline interpolation. Within the CNDO-SCF approximation that neglects overlap in solving the secular equation, $K_{ij}(t) = \langle \phi_i(t) | d\phi_j(t)/dt \rangle$ in Eq. (4) can be ignored. We have examined the effects of $K_{ij}(t)$ on $P_{DA}(t)$ at the extended-Hückel level and found them to be negligible. Given $\mathbf{H}(t)$ for a particular time segment, two C_α -H σ bonds of the backbone are chosen as the D–A pair for the entire time segment (denoted $\phi_D(t)$, $\phi_A(t)$). The initial D–A resonance is achieved by shifting $E_D(0)$ and $E_A(0)$ into the HOMO–LUMO gap, and then setting $|E_D(0) + T_{DD}(0) - [E_A(0) + T_{AA}(0)]| < T_{DA}(0)$ ($T_{KL}(t)$ is given in Eq. (8)) [16–18]. The Schrödinger equation (Eq. (4)) is propagated with a time step of 10^{-3} fs to obtain stable solutions.

3. Results and discussion

A large number of simulations were performed using different MD trajectories and D–A positions. The D–A pairs chosen either belong to the same β -sheet strand (covalent pathways) or to different strands (hydrogen bond pathways), with $10^{-2} \geq \sqrt{\langle T_{DA}^2 \rangle} > 10^{-5}$ eV. $\langle T_{DA}^2 \rangle = (1/T) \int_0^T dt T_{DA}^2(t)$ where $T = 1$ ps. In all simulations, the structural fluctuations do not create resonances between instantaneous bridge eigenstates and $E_D(t)$, $E_A(t)$.

In Fig. 3, we compare typical dynamic- and static-bridge probabilities for time-dependent (top) and static (bottom) E_D , E_A . (a) shows $P_{DA}(t)$ and $P_{DA}^{\text{st}}(t)$, and (b) shows $\mathcal{P}_{DA}(t)$ and $\mathcal{P}_{DA}^{\text{st}}(t)$ for the D,A orbitals C_α -H(Met-121) and C_α -H(Gly-123). In both cases, we use the same MD trajectory with $E_D(0) \simeq E_A(0) \simeq -10$ eV, and $\sqrt{\langle T_{DA}^2 \rangle} \simeq 10^{-3}$ eV. The important observation is that the static-bridge probability deviates from its dynamic-bridge coun-

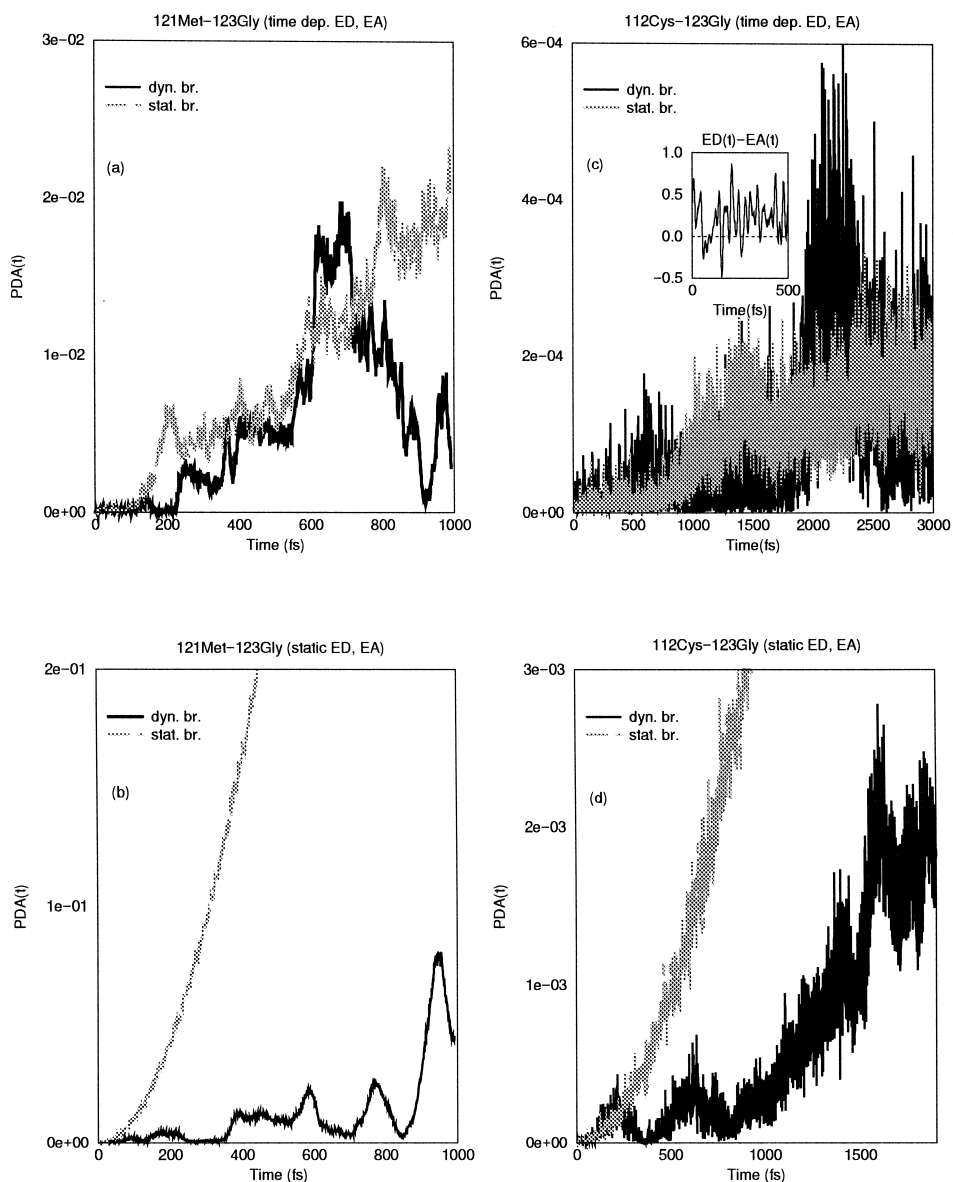


Fig. 3. (a) $P_{DA}(t)$ (dyn. br.) versus $P_{DA}^{st}(t)$ (stat. br.) for time-dependent E_D and E_A , (b) $\mathcal{P}_{DA}(t)$ (dyn. br.) versus \mathcal{P}_{DA}^{st} (stat. br.) for static E_D and E_A . The D,A pair is C α -H(Met-121) and C α -H(Gly-123) with $\sqrt{\langle T_{DA}^2 \rangle} \approx 10^{-3}$ eV. (c) $P_{DA}(t)$ (dyn. br.) versus $P_{DA}^{st}(t)$ (stat. br.) for time-dependent E_D and E_A , (d) $\mathcal{P}_{DA}(t)$ (dyn. br.) versus \mathcal{P}_{DA}^{st} (stat. br.) for static E_D and E_A . The D,A pair is C α -H(Cys-112) and C α -H(Gly-123) with $\sqrt{\langle T_{DA}^2 \rangle} \approx 10^{-4}$ eV. In all cases, $E_D(0), E_A(0) \approx -10$ eV, $\langle E_{\text{homo}} \rangle \approx -11.2$ eV, $\langle E_{\text{lumo}} \rangle \approx 1.5$ eV, with rms deviations ≈ 0.25 eV. Also shown in (c) is $E_D(t) - E_A(t)$ (in units of eV) for a segment of the MD trajectory. Multiple D-A level crossings are visible.

terpart on a fast time scale, approximately 200 fs for the time-dependent E_D , E_A (Fig. 3a), and 40 fs for the static E_D , E_A (Fig. 3b).

Fig. 3c,d shows analogous plots of dynamic- and static-bridge probabilities for a different MD trajectory and a larger D-A separation. The D,A pair

chosen is $C_{\alpha}\text{-H}(\text{Cys-112})$ and $C_{\alpha}\text{-H}(\text{Gly-123})$ with intervening hydrogen bonds. $E_D(0) \approx E_A(0) \approx -10$ eV, and $\sqrt{\langle T_{DA}^2 \rangle} \approx 10^{-4}$ eV. Again, the deviation between the static- and dynamic-bridge probabilities

occurs at short times, approximately 1 ps in Fig. 3c and 250 fs in Fig. 3d. As expected, in all of the above cases, electron transfer is more efficient for the static (resonant) E_D , E_A .

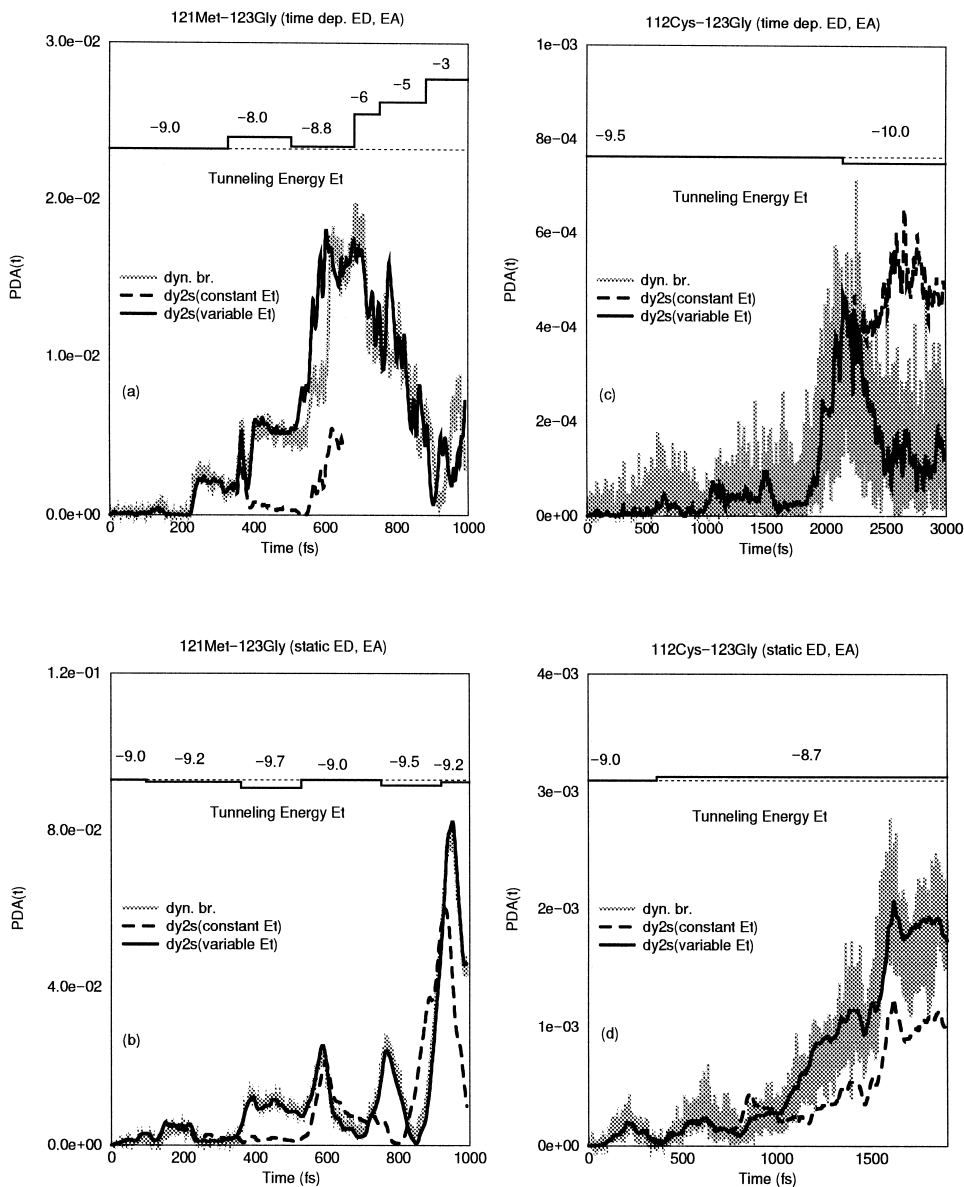


Fig. 4. (a) $P_{DA}(t)$ (dyn.br.) versus $P_{DA}^{dy2s}(t)$ (constant E_{tun}) and $\tilde{P}_{DA}^{dy2s}(t)$ (variable E_{tun}), for the system of Fig. 3a. (b) $\mathcal{P}_{DA}(t)$ (dyn.br.) versus $\mathcal{P}_{DA}^{dy2s}(t)$ (constant E_{tun}) and $\tilde{\mathcal{P}}_{DA}^{dy2s}(t)$ (variable E_{tun}), for the system of Fig. 3b. (c) $P_{DA}(t)$, $P_{DA}^{dy2s}(t)$ and $\tilde{P}_{DA}^{dy2s}(t)$ for the system of Fig. 3c. (d) $\mathcal{P}_{DA}(t)$, $\mathcal{P}_{DA}^{dy2s}(t)$ and $\tilde{\mathcal{P}}_{DA}^{dy2s}(t)$ for the system of Fig. 3d. At the top of each figure we show the time sequence of E_{tun} used in $P_{DA}^{dy2s}(t)$ (a,c), or $\tilde{P}_{DA}^{dy2s}(t)$ (b,d). The initial E_{tun} in the sequence is the value used in $P_{DA}^{dy2s}(t)$ or $\mathcal{P}_{DA}^{dy2s}(t)$

The deviation between the dynamic- and static-bridge probabilities is relevant to the analysis of electron transfer if it occurs prior to thermal relaxation of $E_D(t)$ and $E_A(t)$ from the transition state region. In this case, the static-bridge description is

inadequate and, therefore, the static two-state (T_{DA}) approximation cannot be used. Our simulations show that the dynamic two-state approximation (Eq. (7)) provides a good description of dynamic-bridge tunneling for longer times than the static-bridge proba-

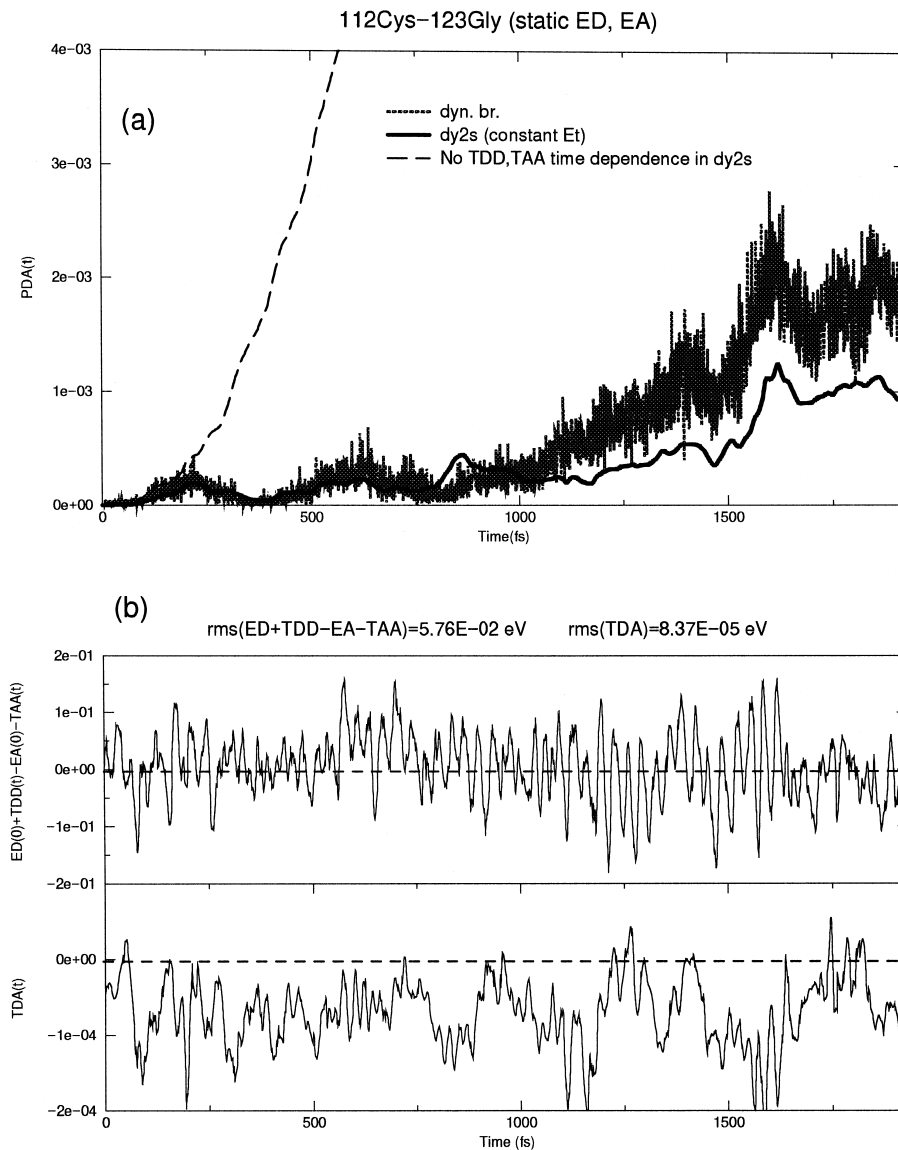


Fig. 5. (a) $\mathcal{P}_{DA}(t)$ (dyn. br.) and $\mathcal{P}_{DA}^{dy2s}(t)$ (constant E_{tun}) of Fig. 4d together with the two-state probability obtained from the following approximation. In the $\hat{H}^{2s}(t, E_{\text{tun}})$ used to compute $\mathcal{P}_{DA}^{dy2s}(t)$, we set $T_{AA}(t) = T_{AA}(0)$, $T_{DD}(t) = T_{DD}(0)$, and retain $T_{DA}(t)$ and its Hermitian conjugate. (b) Plot of the matrix elements of $\hat{H}^{2s}(t, E_{\text{tun}})$ used in $\mathcal{P}_{DA}^{dy2s}(t)$ above. $E_D(0) + T_{DD}(t) - [E_A(0) + T_{AA}(t)]$ (top), $T_{DA}(t)$ (bottom). The rms deviation of $E_D(0) + T_{DD}(t) - [E_A(0) + T_{AA}(t)]$ is greater than the rms deviation of $T_{DA}(t)$ by three orders of magnitude.

bility does. The dynamic two-state approximation should therefore replace the static two-state approximation for the description of tunneling.

In Fig. 4 we compare the dynamic-bridge probabilities of Fig. 3 that were obtained by using the full Hamiltonian of the system ($P_{\text{DA}}(t)$ and $\mathcal{P}_{\text{DA}}(t)$), to the two types of dynamic two-state probabilities obtained from the reduced Hamiltonian $\hat{H}^{2s}(t, E_{\text{tunn}}$) in Eq. (7). Fig. 4a,c are plots of $P_{\text{DA}}(t)$, $P_{\text{DA}}^{\text{dy}2s}(t)$ (constant E_{tunn}) and $\tilde{P}_{\text{DA}}^{\text{dy}2s}(t)$ (variable E_{tunn}), for the D,A pairs and MD trajectories of Fig. 3 and Fig. 4b,d shows $\mathcal{P}_{\text{DA}}(t)$ versus $\mathcal{P}_{\text{DA}}^{\text{dy}2s}(t)$ (constant E_{tunn}) and $\tilde{\mathcal{P}}_{\text{DA}}^{\text{dy}2s}(t)$ (variable E_{tunn}), for the D, A pairs (MD trajectories) of Fig. 3b,d. Superimposed at the top of each graph is the time sequence of E_{tunn} used in $\tilde{P}_{\text{DA}}^{\text{dy}2s}(t)$ (or $\tilde{\mathcal{P}}_{\text{DA}}^{\text{dy}2s}(t)$) to reproduce $P_{\text{DA}}(t)$ (or $\mathcal{P}_{\text{DA}}(t)$). The initial E_{tunn} in each sequence is the value used to compute $P_{\text{DA}}^{\text{dy}2s}(t)$ (or $\mathcal{P}_{\text{DA}}^{\text{dy}2s}(t)$). The energy scale in all E_{tunn} plots is the same.

The main observation in Fig. 4 is that the dynamic two-state probability reproduces the dynamic-bridge N -state probability, for longer times than the static-bridge N -state probability does (shown in Fig. 3). Furthermore, the dynamic two-state approximation with variable E_{tunn} is much better than its constant E_{tunn} counterpart. We have found that the breakdown of the dynamic two-state approximation can be avoided by adjusting E_{tunn} at the right time. A comparison between Fig. 4a and 4b indicates that the necessary adjustments in E_{tunn} for the time-dependent E_{D} and E_{A} , are greater than the corresponding adjustments for the static E_{D} and E_{A} . In Fig. 4a the maximum adjustment per step is 2.8 eV, whereas in Fig. 4b it is 0.7 eV. A similar trend is observed in Fig. 4c,d; the tunneling electron exchanges more energy with its environment when E_{D} , E_{A} , and bridge fluctuate.

Although $T_{\text{DA}}(t)$ in $\hat{H}^{2s}(t, E_{\text{tunn}})$ is essential to the description of the tunneling dynamics (as it represents the effective D–A coupling), the effective diagonal matrix elements $T_{\text{DD}}(t)$ and $T_{\text{AA}}(t)$ are also very important. Fig. 5a shows $\mathcal{P}_{\text{DA}}(t)$ and $\mathcal{P}_{\text{DA}}^{\text{dy}2s}(t)$ (constant E_{tunn}) of Fig. 4d. Superimposed on these two plots is the probability obtained by ignoring in $\hat{H}^{2s}(t, E_{\text{tunn}})$ of $\mathcal{P}_{\text{DA}}^{\text{dy}2s}(t)$ the time dependence of $T_{\text{DD}}(t)$ and $T_{\text{AA}}(t)$ (while retaining that of $T_{\text{DA}}(t)$). The latter probability quickly deviates from $\mathcal{P}_{\text{DA}}(t)$ and $\mathcal{P}_{\text{DA}}^{\text{dy}2s}(t)$, indicating the importance of the effective

diagonal matrix elements in the dynamic two-state approximation. An explanation for this behaviour is given in Fig. 5b where we plot $E_{\text{D}}(0) + T_{\text{DD}}(t) - [E_{\text{A}}(0) + T_{\text{AA}}(t)]$, and $T_{\text{DA}}(t)$ as a function of time. $T_{\text{DD}}(t)$ and $T_{\text{AA}}(t)$ cause a multitude of ‘effective’ D–A level crossings that are absent if these elements are ignored (since the ‘real’ D and A energies are fixed). Level crossings are essential to the description of tunneling dynamics within the two-state approximation.

4. Conclusion

We have shown that the tunneling dynamics of an electron between time-dependent donor and acceptor states that are connected by a fluctuating β -sheet bridge, is very different from the tunneling dynamics through a chemically identical static bridge. The dynamic-bridge ET probability rapidly deviates from its static-bridge behaviour. The time scale of this deviation is the time scale of validity of the static T_{DA} approximation. The dynamic-bridge probability can be approximated for much longer times by use of an effective time-dependent two-state Hamiltonian $\hat{H}^{2s}(t, E_{\text{tunn}})$, where E_{tunn} is also a function of time. The off-diagonal matrix element in $\hat{H}^{2s}(t, E_{\text{tunn}})$, $T_{\text{DA}}(t)$, is the time-dependent analogue of the static T_{DA} , and it describes time-dependent ET pathways. The effective diagonal matrix elements $T_{\text{DD}}(t)$ and $T_{\text{AA}}(t)$, describe effects of the bridge motion on the tunneling dynamics that cannot be included in $T_{\text{DA}}(t)$. When these diagonal elements are added to the real donor and acceptor energies, they change the level crossing dynamics of the effective two-state system. Therefore, their time evolution cannot be ignored.

Acknowledgements

Work supported by the University of Cyprus research program: ‘From Strong Interactions to Molecular Recognition: Theoretical and Computational Studies’. S.S. is indebted to Prof. D.N. Beratan for very helpful discussions.

References

- [1] R.A. Marcus, N. Sutin, *Biochim. Biophys. Acta* 811 (1987) 265.
- [2] M.D. Newton, *Chem. Rev.* 91 (1991) 767.
- [3] J. Jortner, M. Bixon (Eds.), *Advances in Chemical Physics* 106 (1999) 107.
- [4] S. Larsson, *J. Am. Chem. Soc.* 103 (1981) 4043.
- [5] G.W. Canters, E. Vijgenboom (Eds.), *Biological Electron Transfer Chains: Genetics, Composition and Mode of Operation*, Kluwer Academic Publ., The Netherlands, 1998.
- [6] J. Tang, *J. Chem. Phys.* 98 (1993) 6263.
- [7] I.A. Goychuk, E.G. Petrov, V. May, *J. Chem. Phys.* 103 (1995) 4937.
- [8] O. Kühn, V. Rupasov, S. Mukamel, *J. Chem. Phys.* 104 (1996) 5821.
- [9] J. Wolfgang, S. Risser, S. Priyadarshy, D.N. Beratan, *J. Phys. Chem. B* 101 (1997) 2986.
- [10] V.S. Pande, J.N. Onuchic, *Phys. Rev. Lett.* 78 (1997) 146.
- [11] W.B. Davis, M.R. Wasielewski, M.A. Ratner, V. Mujica, A. Nitzan, *J. Phys. Chem. A* 101 (1997) 6158.
- [12] E.S. Medvedev, A.A. Stuchebrukhov, *J. Chem. Phys.* 107 (1997) 3821.
- [13] E.N. Baker, *J. Mol. Biol.* 203 (1988) 1071.
- [14] B.R. Brooks, R.E. Bruccoleri, B.D. Olafson, D.J. States, S. Swaminathan, M. Karplus, *J. Comp. Chem.* 4 (1983) 187.
- [15] F. Weinhold, QCPE Program No. 408.
- [16] S. Skourtis, D.N. Beratan, J.N. Onuchic, *Chem. Phys.* 176 (1993) 501.
- [17] V. Mujica, M. Kemp, M.A. Ratner, *J. Chem. Phys.* 8 (1994) 6849.
- [18] S. Skourtis, S. Mukamel, *Chem. Phys.* 197 (1995) 367.
- [19] J.J. Regan, A.J. Di Bilio, R. Langen, L.K. Skov, J.R. Winkler, H.B. Gray, J.N. Onuchic, *Chem. Biol.* 2 (1995) 489.